ELSEVIER

European Journal of Ultrasound 7 (1998) 73–81

EUROPEAN JOURNAL
OF
ULTRASOUND

Scientific paper

Estimation of acoustical streaming: theoretical model, Doppler measurements and optical visualisation

Andrzej Nowicki *, Tomasz Kowalewski, Wojciech Secomski, Janusz Wójcik

Institute of Fundamental Technological Research, Polish Academy of Sciences, Swietokrzyska 21, 00-049 Warsaw, Poland

Abstract

An approximate solution for the streaming velocity generated by flat and weakly focused transducers was derived by directly solving the Dirichlet boundary conditions for the Poisson equation, the solution of the Navier-Stokes equation for the axial components of the streaming velocity. The theoretical model was verified experimentally using a 32 MHz pulsed Doppler unit. The experimental acoustical fields were produced by three different 4 mm diameter flat and focused transducers driven by the transmitter generating the average acoustic power within the range from 1 μW to 6 mW. The streaming velocity was measured along the ultrasonic beam from 0 to 2 cm. Streaming was induced in a solution of water and corn starch. The experimental results showed that for a given acoustic power the streaming velocity was independent of the starch density in water, changed from 0.3 to 40 grams of starch in 1 l of distilled water. For applied acoustic powers, the streaming velocity changed linearly from 0.2 to 40 mm/s. Both, the theoretical solutions for plane and focused waves and the experimental results were in good agreement. The streaming velocity field was also visualised using the particle image velocimetry (PIV) and two different evaluation methods. The first based on the *FFT*-based cross-correlation analysis between small sections for each pair of images and the second employing the algorithm of searching for local displacements between several images.

Keywords: Doppler; Acoustical streaming; Velocity; Particle image velocimetry

1. Introduction

The acoustic waves which propagate in liquids obey the general laws of hydrodynamics. In a linear medium the dependence between the pressure and the particle velocity is linear; in other words, the acoustic impedance is constant. In a non-linear medium, the impedance varies in time and the acoustic pressure has a constant component and by analogy to electric systems, it may be said that a non-linear medium acts like a pressure

* Corresponding author. Tel.: +48 22 8269841; fax: +48 22 8269815; e-mail: anowicki@ippt.gov.pl

0929-8266/98/$19.00
PII S0929-8266(98)00020-2

rectifier. Waves with finite amplitudes are accompanied by such events as the radiation pressure and streaming.

2. Theory

Nyborg (1965) solved the Navier-Stokes equation with an accuracy up to the second order approximations. Wu and Du (1993) developed the theory of deriving the approximate solution to the Nyborg equation. Adopting relevant assumptions, the authors obtained the Poisson equation as a description of the component v_{2z} of the vector $\boldsymbol{v} = [\boldsymbol{v}_{2r}, \boldsymbol{v}_{2z}]$ of the streaming velocity:

$$V^2 v_{2z} = \frac{1}{\mu c}\frac{\partial I_z}{\partial z} = -\frac{2\alpha}{\mu c} I_z \tag{1}$$

where α is the absorption coefficient, c, the wave propagation velocity in the medium, μ, the shear viscosity coefficient, and I_z, the acoustic intensity along the axis.

Although Wu and Du (1993) undertook to solve Eq. (1) from the beginning, we have applied the general solution including the relevant Dirichlet conditions for the equation of this type.

For the case of a bounded plane wave with a circular section, perpendicular to the propagation axis z, with the radius a, and for a Gaussian beam generated by a circular transducer with the radius a, the following solutions were obtained for the component $\boldsymbol{v}_{2z}(x, y, z)$ of the vector of the streaming velocity v along the beam axis ($x = 0,\ y = 0$).

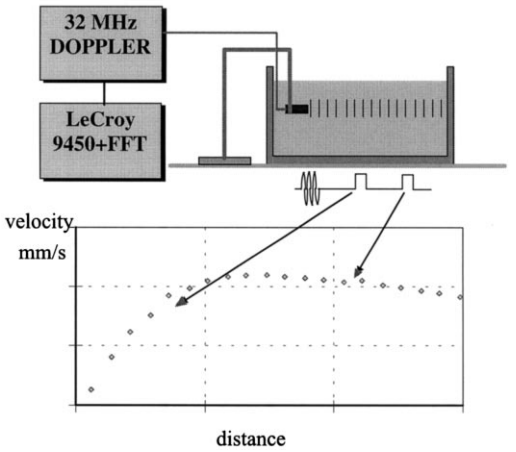

Fig. 1. Block diagram of the Doppler measurement set-up.

(1) Linear (bounded) plane wave

$$v_{2z}(0, 0, z) = \frac{\alpha I_0 a^2}{\mu c}\int_0^{\infty} \mathrm{e}^{-2\alpha a s}\left[\sqrt{1+\left(\frac{z}{a}-s\right)^2} - \sqrt{1+\left(\frac{z}{a}+s\right)^2} + \left(\frac{z}{a}+s\right) - \left|\frac{z}{a}-s\right|\right]\mathrm{d}s \tag{3}$$

where z is the propagation axis, a, the radius of a transducer, α, the absorption coefficient, c, the wave propagation velocity in the medium, μ, the shear viscosity coefficient, and I_0, the acoustic intensity at the transducer face.

(2) A weakly focused beam with a Gaussian intensity distribution

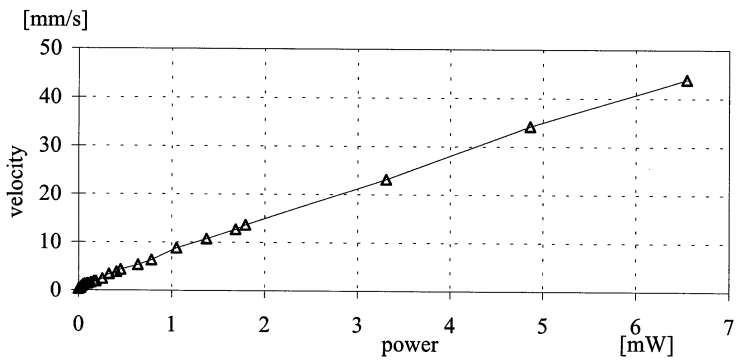

Fig. 2. Streaming velocity in function of the radiated acoustic power; plane 32 MHz transducer (Nowicki et al., 1997).

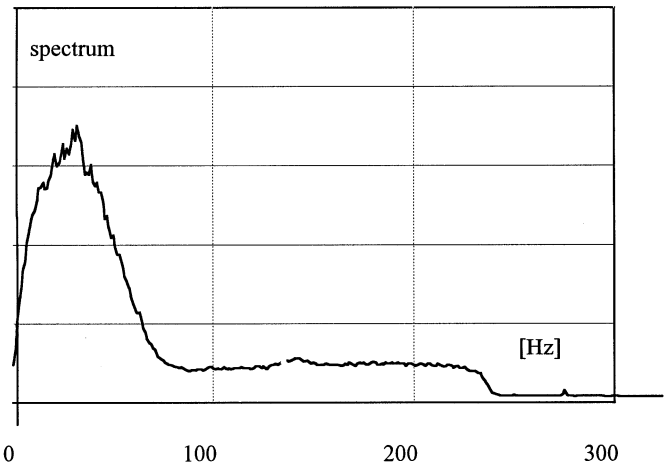

Fig. 3. Doppler spectrum of the streaming velocity measured at the depth of 0.6 mm for plane beam.

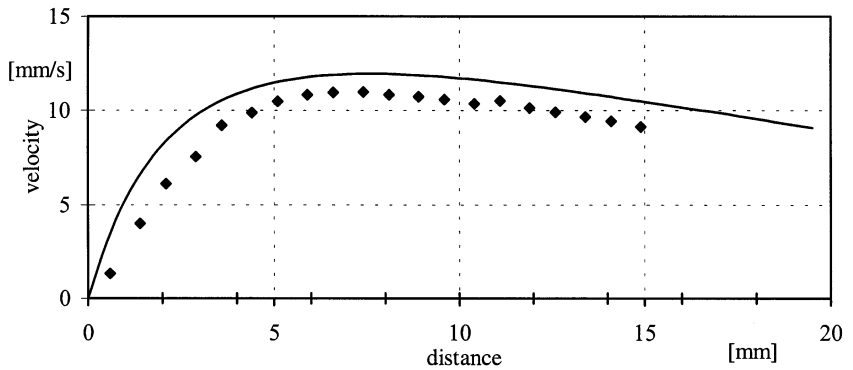

Fig. 4. Streaming velocity vs. distance, plane 32 MHz transducer. The radius of the transducer is equal to 4 mm. The solid line, theoretical calculations, points, experimental results (Nowicki et al., 1997).

$$v_{2z}(0,0,z)=\frac{1}{2}\sqrt{\frac{\pi}{2}}\frac{\alpha I_0 a^2}{\mu c B}\int_0^{\infty}\sqrt{A(z')}\,\mathrm{e}^{-2\alpha z'}\times\left[\mathrm{e}^{(2A(z')/a^2)(z-z')^2}\,erfc\left[\frac{\sqrt{2A(z')}}{a}(z-z')\right]\times\mathrm{e}^{(2A(z')/a^2)(z+z')^2}\,erfc\left[\frac{\sqrt{2A(z')}}{a}(z+z')\right]\right]\mathrm{d}z' \tag{4}$$

where

$$A(z)\equiv\frac{BRF(R)}{z-F(R))^2+C(R)},\quad F(R)\equiv\frac{r_0^2R}{r_0^2+(BR)^2},\quad C(R)\equiv F(R)[R-F(R)],$$

R is the geometrical focal length of the acoustic lens, $F(R)$ is the physical focal length (the position of the maximum of the field intensity distribution), $r_0=(1/2)\mathrm{ka}^2$, B is a constant related to the Gaussian beam and equals one on the transducer surface ($z=0$).

In their computer calculations the authors used the numerical approximation of the function $erfc(x)$ (Abramowitz and Stegun, 1968):

$$erfc(x)=efc(x)\,\mathrm{e}^{-x^2}+\varepsilon(x),\quad |\varepsilon(x)|\le 1.5\cdot 10^{-7},$$
$$efc(x)\equiv\sum_{n=1}^{5}p_n f(x)^n,\quad f(x)=\frac{1}{1+px} \tag{5}$$

$p=0.3275911$, $p_1=0.254829592$, $p_2=-0.284496736$, $p_3=1.421413741$, $p_4=-1.453152027$, and $p_5=1.0614005429$.

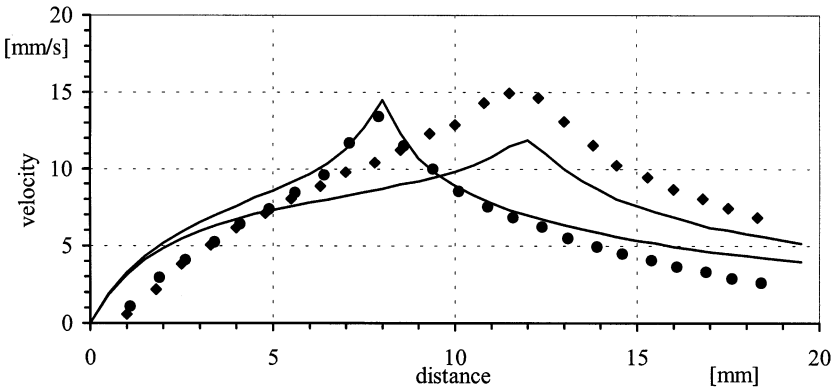

Fig. 5. Streaming vs. distance; focused transducers, focal distance = 8 and 12 mm, radius of the transducer is equal to 4 mm. The solid line, theoretical calculations, points, experimental results (Nowicki et al., 1997).

Substituting approximation (5) into (4), the following expression, convenient for computer calculations is obtained.

$$v_{2z}(0,0\,z)=\frac{\alpha I_0 a\sqrt{\pi}}{2\sqrt{2}\mu cB}\int_0^{z+z_g}\sqrt{A(z')}\,\mathrm{e}^{-2\alpha z'}\left\{efc\left[\frac{\sqrt{2}A(z')|z-z'|}{a}\right]-efc\left[\frac{\sqrt{2}A(z')(z+z')}{a}\right]\right\}\mathrm{d}z' \tag{6}$$

where z_g depends in fact on z and the properties of the function $\sqrt{A(z')}\,\mathrm{e}^{-2\alpha z'}$. In our calculations for $z \le 3R$ we adopted $z_g = 3R$. For $z \ge 4R$ it is sufficient to adopt $z_g \cong R$. For large z, but ones smaller than $1/\alpha$, z_g may be determined using the relation $z + z_g < \max[1/\alpha,\ 2R)]$.

It was assumed in the calculations that in water $\alpha = 2.53 \cdot 10^{-16} f^2$ Np/cm Hz^2 and $\mu = 0.01$ Poise.

3. Methods and results

3.1. Measuring system

The streaming was measured using a Doppler ultrasound blood flowmeter. The transmitter generated a 32 MHz bursts, lasting 0.5 μs with the repetition frequency equal to about 31 kHz. The backscattered signal was received in a gate of 0.5 μs duration and variable delay. The bandwidth of the receiver was extended from the DC up to 4 kHz. The backscattered Doppler signal was analysed using the digital oscilloscope LeCroy 9450A including FFT spectrum analyser. Up to 100 successive Doppler spectra were averaged (frequency resolution was 0.1–1 Hz). Three different flat and focused (focused at depths of 8 and 12 mm) lithium niobate 4 mm diameter transducers were examined. The estimated power was about 1.4 mW for each of the three transducers. Fig. 1

3.2. Measurements

Streaming was measured in a rectangular container filled with a corn starch suspension in distilled water. The system consisted of a Doppler flowmeter and an ultrasonic transducer working at 32 MHz, submerged in a container with water. The Doppler signal was analysed using the oscilloscope LeCroy 9450A with an FFT analysis module. The maximum flow velocity was determined as the maximum frequency below which 90% of the power of the Doppler signal lies. The streaming velocity increased linearly with the power transmitted in the range between 0.001 to 6 mW. The correlation coefficient was $R = 0.9992$. (see Figs. 2 and 3).

Fig. 4 shows the streaming velocity for a plane transducer. Fig. 5 shows the streaming velocities for transducers focused at 8 and 12 mm depths, respectively.

The flow velocity changes were measured for different densities of the starch suspension in water. It was found that for densities between 0.3

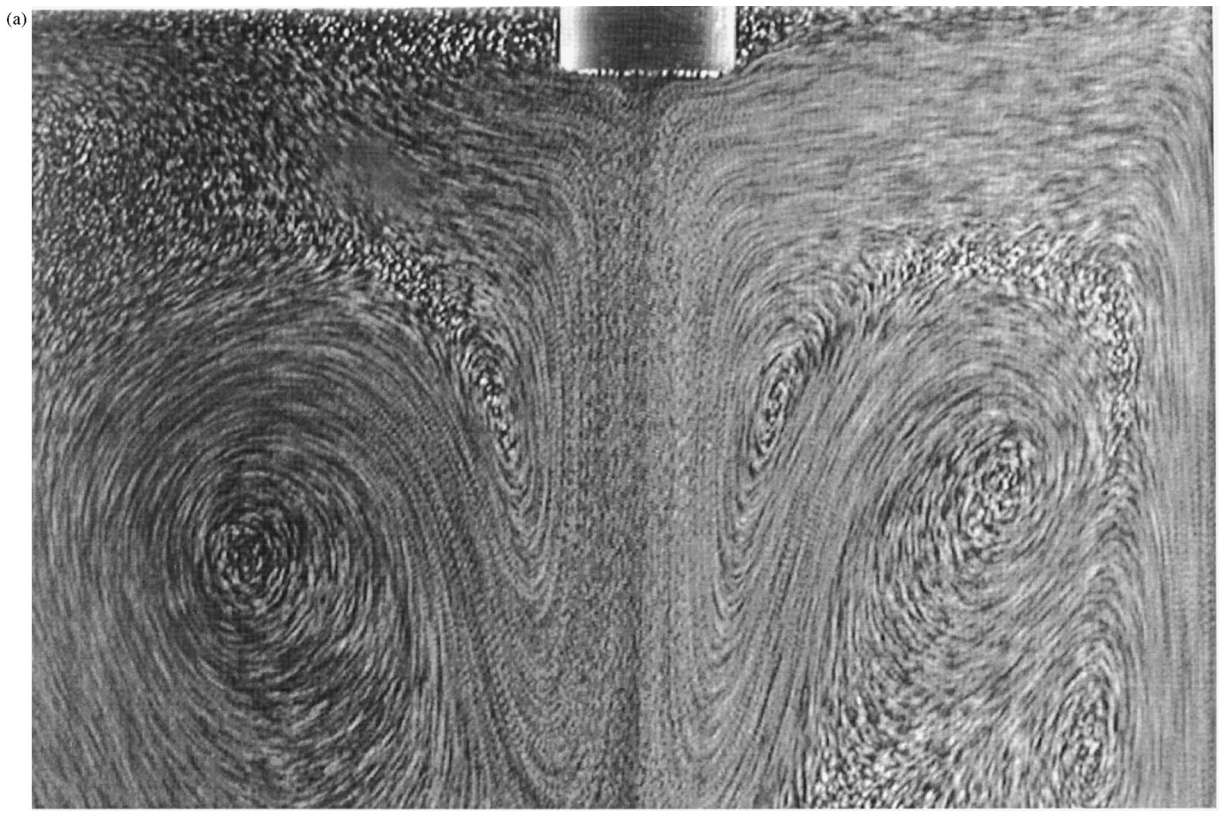

Fig. 6. Visualisation of acoustic streaming, ten superimposed images taken at 200 ms interval. (a) Plane wave transducer, (b) focused transducer.

and 40 g/l the streaming velocity hardly varied. The maximum deviation from the mean value was -5.3%. The S.D./mean ratio $= 0.07$. For a higher starch concentration than 40 g/l, the streaming velocity fell; it was probably caused by higher viscosity of the suspension.

4. Flow visualisation and measurement of the velocity field

An experimental set-up used for measurements consisted of a $64 \times 64 \times 90$ mm rectangular box, special constructed halogen tube illumination, and a CCD video camera. As a flow medium distilled water and two aqueous solutions of glycerine (40 and 80% per vol.) were used. The flow was seeded with a very dilute (below 0.1%) fine pine pollen powder. The cavity walls were made of glass with the top side left opened. Ultrasonic transducers used were immersed at the centre of the top surface, approximately 4 mm deep into the liquid. Two 32 MHz transducers generating the plane and focused beams (12 mm focal distance) were used. The flow was observed at the vertical cross sections of the cavity using a light sheet technique. The flow images of 768×512 pixels were acquired by an 8-bit frame grabber (VFG-ITI). Transient development of the flow was recorded using short series of images acquired every 30–60 s and stored on the hard disk of the computer for later evaluation.

The 2-D velocity vector distribution was measured by particle image velocimetry (PIV). By this method, the motion of the scattering particles observed in the plane of the illuminating light sheet can be analysed. Each of the images shows a relatively dense cloud of single illuminated parti-

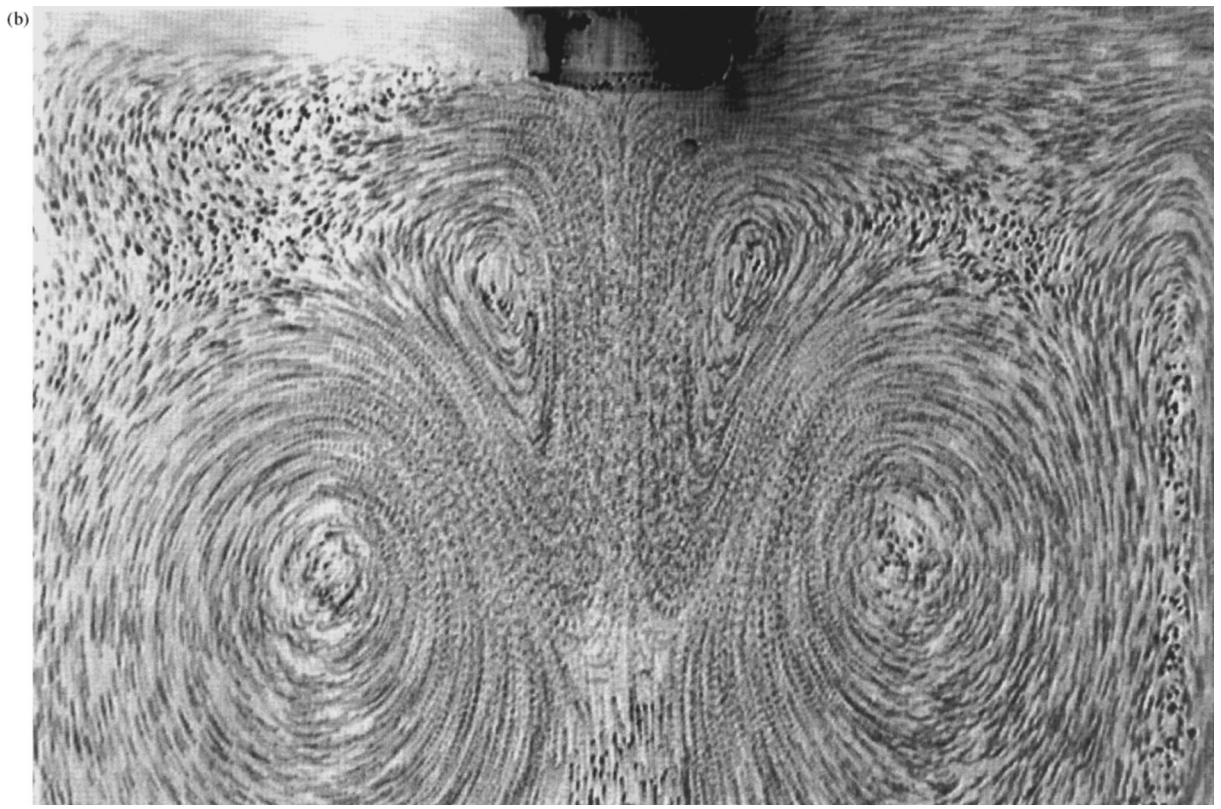

Fig. 6. (*Continued*)

cles. A sequence of two or more separately captured digital images taken at a constant time interval (typically 200 ms) were used to evaluate the magnitude and direction of the velocity vectors. Two evaluation methods were used. The first one is based on the FFT-based cross-correlation analysis between small sections (interrogation windows) performed for each pair of images (Hiller et al., 1993). The average particle displacement during given time interval determines the velocity vector representing analysed section. By moving step by step interrogation widow across the image about 1000 vectors per one pair of images were obtained. The spatial resolution of the method is limited by minimum amount of tracers to be present in the interrogation window. In practice, the minimum window size was 32×32 pixels. The second method, recently developed DP-PIV 'optical flow' based technique, searches for local displacements between several images (Quenot et al., 1997). It allowed to improve accuracy and to obtain dense velocity field (displacement vector for each image pixel).

Several images recorded periodically within a given time interval were added in the computer memory in order to obtain a general view of the flow pattern. Displayed images are similar to the multiexposed photographs, showing the flow direction and its structure (Fig. 6). The generated flow is strongly 3-D but only its central cross-section was recorded. Observed asymmetry of the flow pattern indicates effects of the 'third' velocity component, shifting the main flow stream out of the symmetry plane.

The acoustic field radiating from the transducer generated flow in the cavity. This was observed for the pure water and 40% glycerol solution. For highly viscous 80% glycerol the effect of the acoustic field was invisible. The onset of the flow was recorded. After switching the power on, al-

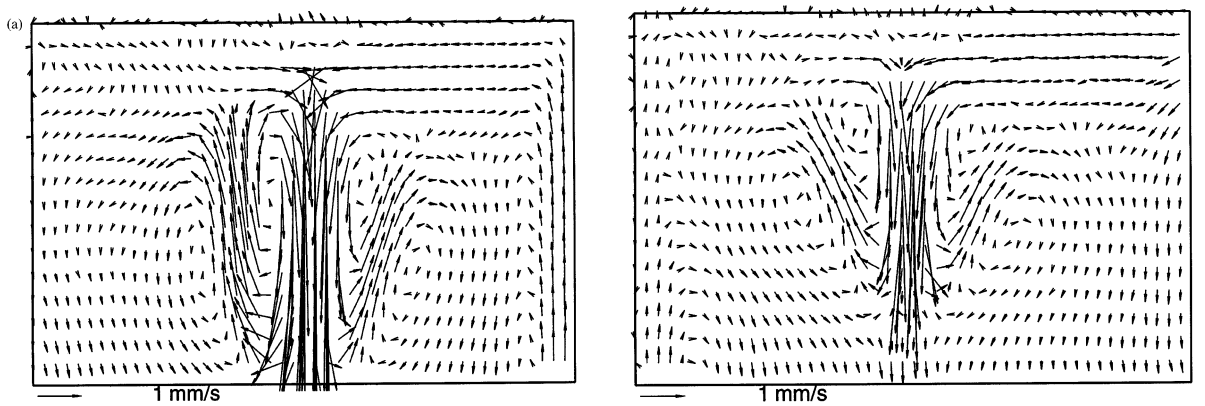

Fig. 7. Measured velocity field in the centre cross-section by DP-PIV method; only every 16th vector displayed. (a) Plane beam, horizontal size 62 mm, (b) focused beam, horizontal size 53 mm.

most uniform flow stream along the axis of the transducer was observed. The flow originated from the transducer, pointing down into the cavity bottom. Subsequent flow interaction with the side walls and the liquid surface induced reverse flow, transporting liquid back to the surface. Finally complex interaction of the main flow stream with the reverse flow established an regular flow pattern, with the characteristic double-vortex structure. Typical transition time was about 3 min for water as a flow medium.

A different flow pattern was observed for the 40% glycerine solution. For this case, it took up to about 5 min after switching the acoustic field on before a steady circulation was established in the near transducer region (about 15 mm below the transducer face), where the spiralling motion transported liquid down along the transducers axis and back to the surface. The maximum flow velocity was about 2 mm/s. This circulation induced very slow secondary recirculation in the cavity.

The effect of the acoustic field characteristic was investigated replacing plane beam transducer with the focused one. The flow patter for both cases differed mainly in details. Its main feature exhibits the main portion of the fast flow streaming pointing down. The example of the velocity profiles extracted along the transducer axis and perpendicularly to it illustrate main differences in flow characteristics (Figs. 7 and 8).

5. Conclusions

The streaming velocities generated by plane and weakly focused ultrasonic heads were calculated. The measured velocity changes as a function of depth confirm well the theoretical calculations for all the three heads. Good quantitative agreement was obtained between the measured streaming velocities and those calculated theoretically. The latter were modified with respect to the solution of the Poisson equation given earlier by Wu and Du. The slight differences are probably caused by the inaccuracy of estimation of the maximum Doppler frequency and the impossibility of accurate measurement of the real acoustic power radiated by transducers in the high frequency range. The measurements for the frequency of 32 MHz indicated a linear dependence of the streaming velocity on the acoustic power. It may be assumed that the addition of starch did not affect the streaming velocity measurements for no changes were found in the measured velocities with percentage variations of the starch content in the suspension.

Given the measurement repeatability and accuracy it may be hoped that in the future the streaming velocity measurement can be applied in evaluating the acoustic power radiated by a transducer. This method may be used to measure

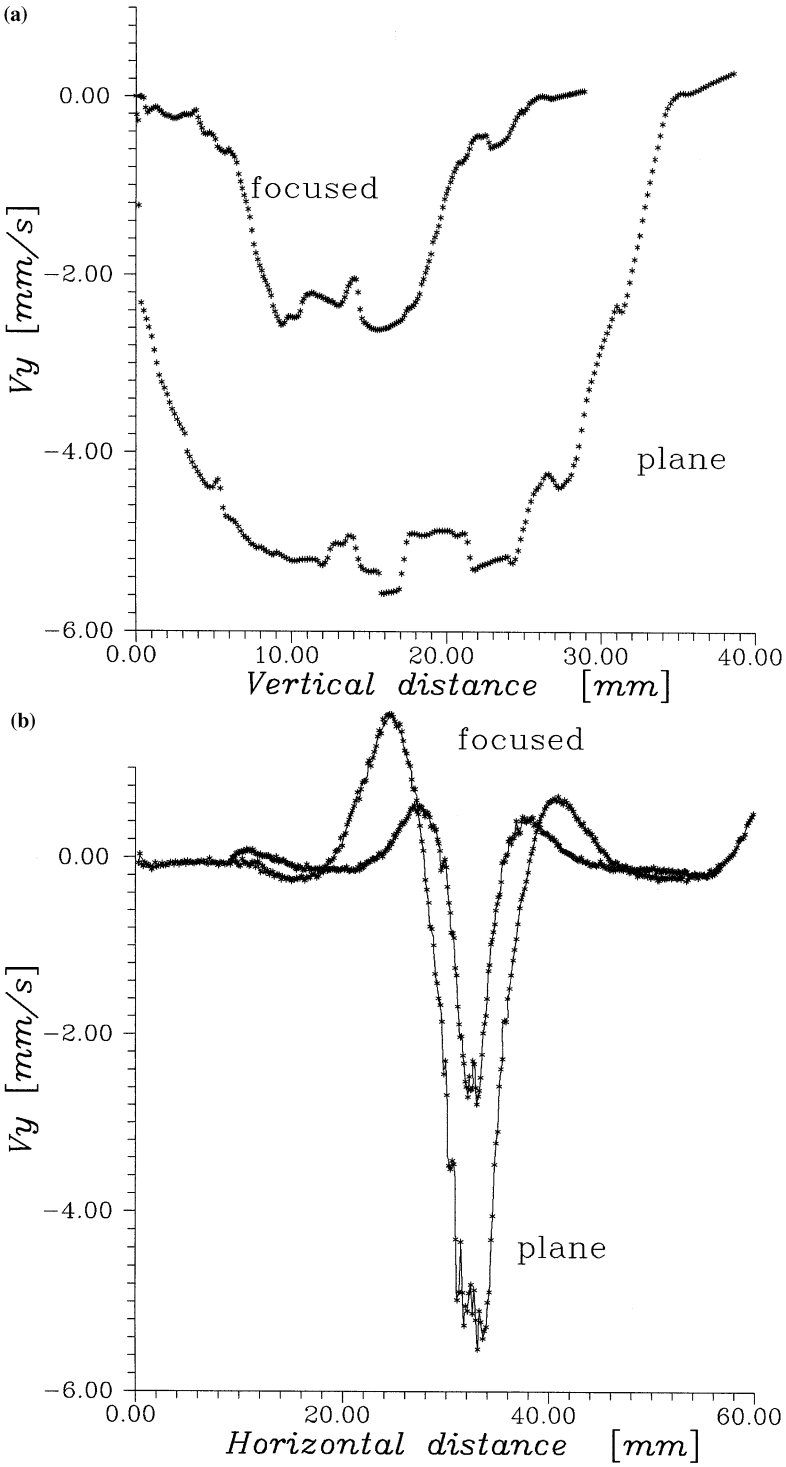

Fig. 8. Velocity profiles extracted from the PIV measurements. (a) Vertical velocity component along transducer axis, distance measured from the transducer external surface, (b) vertical velocity component along horizontal line, passing maximum value (approximately 17 mm from the plane transducer and 13 mm from the focused one).

the acoustic power of ultrasonographic probes meant for medical diagnostics.

The digital flow images demonstrated the main 2-D characteristics of the acoustic steaming generated for the plane and focused beam. The PIV and DP-PIV evaluation of the flow images gave us full plane velocity vector fields, allowing quantitative analysis of the observed flow.

The quantitative results obtained with PIV are not to be directly compared to the ones measured with Doppler. The acoustic intensities used for PIV were not calibrated as the visualisation was intended to be to be the pilot study enhancing the understanding of the streaming phenomena associated with the fluid flow generated by the acoustic radiation force

References

Abramowitz M, Stegun IA, editors. Handbook of Mathematical Functions. New York: Dover, 1968.

Hiller WJ, Koch St, Kowalewski TA, Stella F. Onset of natural convection in a cube. Int J Heat Mass Transf 1993;36:3251–63.

Nowicki A, Secomski W, Wójcik J. Acoustic streaming: comparison of low amplitude linear model with streaming velocities measured by means of 32 MHz Doppler. Ultrasound Med. Biol. 1997;23(5):783–91.

Nyborg WL. Acoustic streaming. In: Mason WP, editor. Physical Acoustics, IIB. New York: Academic Press, 1965:265–331.

Quenot G, Pakleza J, Kowalewski TA. Particle Image Velocimetry with Optical Flow (submitted).

Wu J, Du G. Acoustic streaming generated by focused Gaussian beam and finite amplitude toneburst. Ultrasound Med. Biol. 1993;19(2):167–76.